

Molecular simulations of crazes in glassy polymers under cyclic loading

Tobias Laschuetza,^{*,†} Ting Ge,[‡] Thomas Seelig,[†] and Joerg Rottler^{¶,§}

[†]*Institute of Mechanics, Karlsruhe Institute of Technology, Kaiserstrasse 12, 76131
Karlsruhe, Germany*

[‡]*Department of Chemistry and Biochemistry, University of South Carolina, Columbia,
South Carolina 29208, United States*

[¶]*Quantum Matter Institute, University of British Columbia, Vancouver BC V6T 1Z4,
Canada*

[§]*Department of Physics & Astronomy, University of British Columbia, Vancouver BC V6T
1Z1, Canada*

E-mail: tobias.laschuetza@kit.edu

Abstract

We study with molecular dynamics simulations of a generic bead-spring model the cyclic crazing behaviour of glassy polymers. The aim is to elucidate the mechanical response of sole fibrillated craze matter as well as its interaction with bulk material. The macroscopic stress response exhibits a hysteresis, which is quasi stationary after the first cycle and largely independent of deformation rate and temperature. It results from a complex interplay between constraints imposed by the entanglement network, pore space and pore space closure. Once the craze fibrils are oriented, stretching of the covalent backbone bonds leads to a rapid stress increase. In the initial stages of unloading, a loss in entanglement contact yields a quick stress relaxation in the backbone. During unloading, the craze fibrils undergo a rigid body (i.e. stress-free) folding motion due to the surrounding pore space, so that the structural behaviour of craze fibrils during unloading is most accurately described as string-like. The reloading response depends significantly on the degree of pore space closure and the enforced intermolecular interaction during unloading. It ranges from a linear stress increase to a re-cavitation

with a re-drawing response. Compared to the bulk stiffness, the craze stiffness is two orders of magnitude lower and as a result, the macro response of coexisting craze and bulk matter is governed by the sole fibrillated craze matter.

1 Introduction

Crazing refers to the dilatant process of localized formation and growth of crack-like defects in glassy thermoplastic polymers. A craze consists of fibrillated matter with an interconnected void space. The several tens of nanometre thick fibrils can grow up to a few micrometers in length by drawing in surrounding bulk material from the so-called active zone.¹ This process is of technical importance since, unlike cracks, craze fibrils enable a considerable load transfer between the craze surfaces and substantially enhance the fracture toughness. Therefore, much research has been devoted to understanding the governing mechanisms, cf. reviews in,²⁻⁵ which includes theoretical studies on a continuum scale, e.g.,⁶⁻¹² as well as on a molecular scale, e.g.¹³⁻²⁵ However, the focus of those theoretical studies is limited to monotonic loading conditions. In contrast, extensive experimental research for cyclic (especially fa-

tigue) loading exists, cf. reviews in,^{26–28} providing insight into very interesting fracture processes for several glassy polymers and at several loading amplitudes: For instance, at low loading amplitudes, Skibo et al.²⁹ observed discontinuous crack growth, which was attributed to craze thickening resulting from a competition of fibril drawing and fibril creep deformation by Könczöl et al.³⁰. An increase in loading amplitude may give rise to the formation of shear bands and their interaction with crazes, leading to discontinuous epsilon-shaped fatigue cracks as studied by Takemori²⁸. Yet, the involved length scales pose difficulties to explore the driving mechanisms by solely relying on experiments and without theoretical analyses based on a physically motivated craze model. For this purpose, a continuum micromechanical model was recently developed³¹ focusing on the cyclic response of craze matter. The model describes the structural response of craze fibrils as string-like and accounts for viscoplastic fibril drawing and viscoelastic fibril deformation, where the latter is motivated by experimental observations.^{32,33} It is designed to be employed as a traction separation law in a mode I boundary value problem to investigate cyclic craze and crack growth. The continuum scale also allows to account for inelastic shear yielding in the surrounding bulk, which enables the analysis of its competition with crazing. However, the craze model suffers from two shortcomings arising from a general knowledge gap of the cyclic craze response: On the one hand, the structural behaviour of craze fibrils during unloading is uncertain. The correct structural behaviour is important since it impacts the pictures of the damage mechanism during cyclic (fatigue) loading. On the other hand, there is a lack in detailed mechanical knowledge regarding the response of craze deformation for a broad range of loading conditions.

In this paper, the response of a craze under cyclic loading is studied based on molecular dynamics simulations of a coarse-grained bead-spring model. In the past, this approach has yielded valuable insight into many molecular scale mechanisms of crazing in particular the ones concerning the entanglement net-

work. General studies of craze nucleation,¹⁶ craze fibril drawing,^{13,14,19,20} and craze fracture¹⁵ in linear flexible polymers were extended to nanocomposites,¹⁸ void nucleation,¹⁷ semi-flexible and stiff polymers,^{24,25} and assessed the role of the entanglement network in setting the craze extension ratio.^{22,25} Recent simulations have gone beyond the generic coarse-grained bead-spring model and used a scale-bridging approach to simulate craze formation in polystyrene.²³ Contrary to the energy landscape and stress level, the central role of the entanglement network in controlling the structural features of craze fibrils is independent of the degree of coarse graining.

The aim in this work is twofold: First, to the knowledge of the authors, molecular dynamics simulations have not yet been employed to study the cyclic response of fibrillated craze matter. The access to molecular scale details allows the simulations to establish the microscopic picture, which is often assumed in micromechanical models but is difficult to evaluate experimentally. Therefore, this study aims to elucidate the mechanical behaviour under cyclic loading and the underlying mechanisms leading to the macroscopic response. To this end, different loading conditions are analysed for sole fibrillated craze matter as well as for systems where bulk and craze matter coexist. The latter is of interest, since crazing is a transient process which gains particular relevance during cyclic loading where, for instance, fibril drawing takes place over multiple cycles. A further focus concerns the structural behaviour of craze fibrils during unloading and whether it can be characterised as string-like. Second, findings from this study aim to be transferred as a bottom-up approach to larger scale models to create, for instance, a molecular dynamics informed continuum model.

The presented paper is outlined as follows: In section 2, the computational methods featuring the model, the system setup and the crazing simulation are detailed. The results are presented in section 3 comprising the cyclic response of sole fibrillated craze matter (subsection 3.1) as well as the cyclic response of co-existing craze and bulk material for different

craze-bulk compositions (subsection 3.2). Concluding, the key findings are summarised in section 4.

2 Model and methods

The generic bead-spring model³⁴ is employed to study the cyclic craze response. The model setup is consistent with previous studies on crazing, e.g.,^{13–16,21,22} and is briefly summarised: Each polymer is modelled as a linear chain of N spherical monomers with a mass m . Non-bonded monomers separated by the distance r interact via the truncated and shifted 6-12 Lennard-Jones (LJ) potential

$$U_{\text{LJ}}(r) = 4u_0[(a/r)^{12} - (a/r)^6 - (a/r_c)^{12} + (a/r_c)^6] \quad (1)$$

for $r \leq r_c$ and with a cutoff radius $r_c = 1.5a$. The results are expressed in terms of Lennard-Jones units, featuring the characteristic length a , energy scale u_0 and a characteristic time $\tau = a\sqrt{m/u_0}$. The bonded monomers interact via an attractive finitely extensible nonlinear elastic (FENE) potential with a purely repulsive second Lennard Jones term ($r_c = 2^{1/6}a$)

$$U_{\text{FENE}}(r) = -\frac{1}{2}kR_0^2 \ln[1 - (r/R_0)^2] + 4u_0[(a/r)^{12} - (a/r)^6] \quad (2)$$

with the parameters $R_0 = 1.5a$ and $k = 30u_0/a^2$, allowing entanglements to form.³⁴ Chain scission is not considered, since the focus lies on cyclic loading resulting in stress states lower than necessary for chain scission to occur.¹⁶

The system comprises $M = 1800$ chains where each chain consists of $N = 500$ beads with an average entanglement length of $N_e \approx 80$ beads. Simulations are performed with the LAMMPS molecular dynamics code,^{35,36} where periodic boundary conditions are employed along all three directions.

The melt state was constructed by generating random-walk coils with a subsequent equilibration with $r_c = 1.12a$ at temperature $T = 1u_0/k_b$. To facilitate equilibration, a double bridging algorithm³⁷ is utilized. The temperature was controlled via a Nosé-Hoover thermostat with a damping rate $1\tau^{-1}$. While retaining the volume, the equilibrated system is then quenched with $r_c = 1.5a$ to $T = 0.49u_0/k_b$, leading to zero pressure. Further quenching

to the final target temperature $T = 0.1u_0/k_b$ takes place at zero pressure by using a Nosé-Hoover barostat with a damping rate $0.1\tau^{-1}$. The quenched system has initial box dimensions $L_{x0} = 94.3a$ and $L_{y0} = 55.8a$ in lateral direction and $L_{z0} = 167.3a$ in axial direction. All directions sufficiently exceed the end-to-end distance of the chains, which reduces finite size effects.^{16,38} The larger box length along the z-direction minimises further the effects of the finite box size on the coexistence of the craze fibrils and un-crazed regions. L_{z0} being larger than the active zone size allows better separation of the craze fibrils from the active zone at the same axial stretch $\lambda_z = L_z/L_{z0}$, which is measured with respect to the isotropic glass. The box sizes in the periodic x- and y-directions are reduced compared to L_{z0} , so the simulations with the same number of degrees of freedom can focus on the more interesting z-direction.

Following previous studies, e.g.,^{15,16,22,23} crazing is induced by subjecting the system to an affine uniaxial deformation along the z-axis, i.e. lateral stretches $\lambda_x = \lambda_y = 1$, while λ_z is prescribed via a constant material strain rate $\dot{\lambda}_z = \dot{u}/L_{z0} = 2.6 \cdot 10^{-4}\tau$. To simulate cyclic loading conditions, a bi-linear loading/unloading program is imposed by simply switching the velocity direction upon reaching the maximum stretch $\lambda_{z,max}$, leading to the loading period T_p . Throughout the loading program, a Nosé-Hoover thermostat with a damping rate $1\tau^{-1}$ is applied to the lateral velocities to maintain a constant temperature.

To study the cyclic response of sole craze material in subsection 3.1, the isotropic glass is deformed to $\lambda_{z,max} = 10$. This ensures complete conversion of bulk material into fibrillated craze matter, which takes place when the deformation reaches approximately the extension ratio λ_c (i.e. $\lambda_z \approx \lambda_c = \rho_b/\rho_c$), describing the ratio of bulk ρ_b and craze density ρ_c . It also avoids the deformation state where chain breakage occurs (cf.¹⁶). In subsection 3.2, the bulk-craze interaction for different bulk-craze compositions is studied by varying $\lambda_{z,max}$. To analyse a broad response range, the unloading magnitude $\lambda_{z,u}$, i.e. the stretch to which the system is unloading, is varied in both studies. In all considered

scenarios, the cycle count and the cycle time $\tau_c = \tau/T_p$ commences upon reaching $\lambda_{z,max}$ for the first time after loading from the isotropic glass.

3 Results

3.1 Cyclic response of fibrillated craze matter

We first aim to elucidate the mechanical response of sole craze matter by focusing on the macroscopic behaviour throughout the loading cycles and thereafter analysing the underlying mechanisms. Figure 1 presents the macroscopic response of fibrillated craze matter under cyclic loading for three simulations to $\lambda_{z,u} = 1$ (dash-dotted line), $\lambda_{z,u} = 2$ (dashed line) and $\lambda_{z,u} = 5$ (solid line). The deformation controlled cyclic loading program is shown in Figure 1(a), and the corresponding macroscopic axial stress σ_z as function of the macro stretch λ_z is depicted in Figure 1(b). The grey dotted line represents the initial response of the isotropic glass during craze formation and growth, featuring an elastic stress increase, the subsequent stress drop during cavitation, as well as a constant stress plateau as craze fibrils are drawn from the bulk. This monotonic crazing process has already been thoroughly studied, e.g.^{13,15,16,22} Here we are interested in the mechanical response of the craze (fibrils) under cyclic loading (black lines). To provide a better visualisation, Figure 1(c) shows a zoom of the stress-stretch response (red box in Figure 1(b)), and the arrows in Figure 1(c) show the loading direction. The colour coding and the roman numerals indicate different craze stages.

Before discussing the different stages of the craze deformation cycle, several key features are briefly summarised. During unloading from $\lambda_{z,max} = 10$ (indicated by the vertical arrow in Figure 1(c)), the craze first exhibits a rapid stress decline which transitions into a long, quasi-stress free contraction of the craze (orange line). When the stretch is reduced below $\lambda_{z,u} < 2.5$, the quasi stress-free contraction becomes compressive, and the magnitude

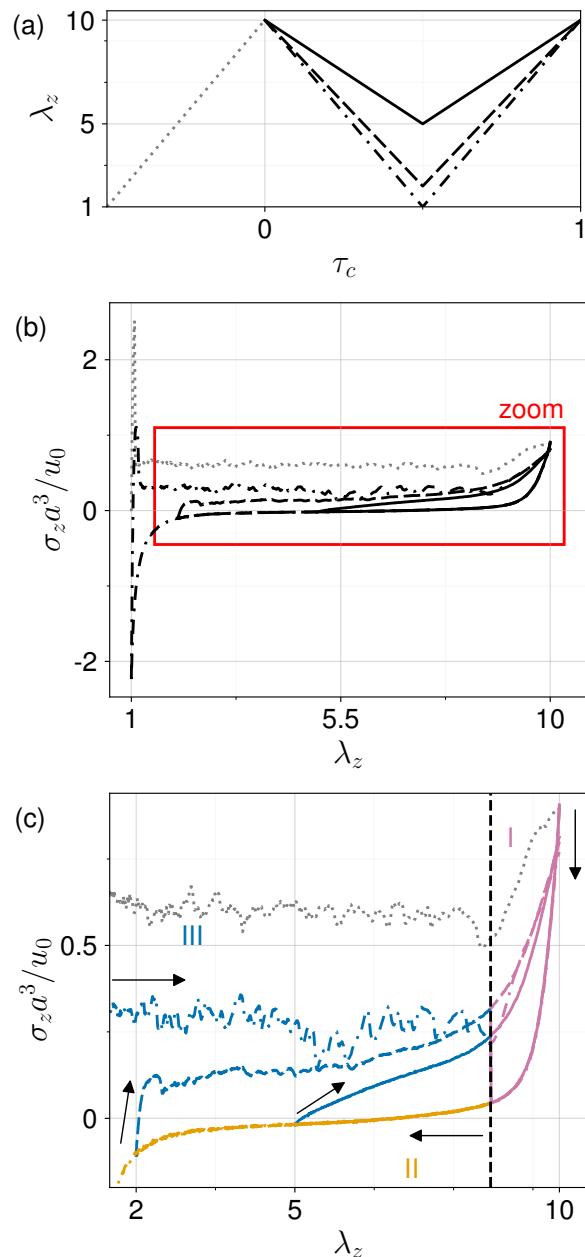


Figure 1: Mechanical response during initial craze formation (grey dotted line) and subsequent cyclic loading (black lines) to various unloading stretches of $\lambda_{z,u} = 1$, $\lambda_{z,u} = 2$ and $\lambda_{z,u} = 5$, represented by black dash-dotted, dashed, and solid lines, respectively. (a) Schematic loading program, (b) axial stress σ_z as function of axial stretch λ_z with red box indicating zoom shown in (c). The arrows and colour coding in panel (c) show loading direction and different craze stages, respectively. The latter are described in the text.

of σ_z significantly rises as λ_z approaches $\lambda_z = 1$ (dash-dotted line), i.e. the macroscopically un-

deformed state of the initial isotropic glass. In that particular case, σ_z increases rapidly during reloading and the craze exhibits what appears to be re-cavitation and re-yielding, while both stress magnitudes remain below the cavitation and drawing stresses during the initial craze creation (grey dotted line). By contrast, for the case of $\lambda_{z,u} = 2$ (dashed line) and $\lambda_{z,u} = 5$ (solid line), the craze exhibits a plateau stress and a linear increase, respectively, during reloading (cf. blue dashed and solid line in Figure 1(c)). Around $\lambda_z \approx \lambda_c$, which is indicated by the vertical line in Figure 1(c), the stress rapidly grows and the response becomes nearly independent of $\lambda_{z,u}$. Moreover, it is notable that all load program variations lead to a hysteresis, which appears to be neither a thermally activated nor a rate-dependent process and relatively stationary after the first cycle (cf. Figure S1 and Figure S2 in the supporting information).

To analyse the driving mechanisms leading to the hysteresis, it is beneficial to distinguish between different craze stages during the deformation cycle. As aforementioned, the stages are represented by the colour-coding and the roman numerals in Figure 1(c) and can be summarised as follows:

- Stage I (magenta): Stretching and unloading of highly oriented craze fibrils. This is labelled here as first stage, since the response is essentially independent of the previous loading history.
- Stage II (orange): Quasi stress-free contraction of the craze with a transition to compression around $\lambda_z = 2.5$.
- Stage III (blue): A reloading response which depends on $\lambda_{z,u}$ and exhibits either a re-yielding ($\lambda_{z,u} \leq 2$) or a linear ($\lambda_{z,u} \geq 5$) behaviour.

To further enhance the understanding, animations (created with OVITO³⁹) of the three simulations are provided in the supporting information.

The further analysis focuses on the 1st cycle as defined in Figure 1(a), if not indicated otherwise.

3.1.1 Mechanics during stage I

The mechanics in stage I are discussed first while focusing on the mechanisms leading to the rapid stress increase during reloading, and the difference between loading and unloading that results in the hysteresis. The former is investigated through a decomposition of σ_z into its intramolecular $\sigma_{z,b}$ and intermolecular $\sigma_{z,p}$ contributions, as shown in Figure 2 for $\lambda_{z,u} = 5$. Since the kinetic contribution is small in the glass, it is omitted here. Stress decompositions for the cases $\lambda_{z,u} = 2$ and $\lambda_{z,u} = 1$ are shown in Figure S3 and exhibit qualitatively similar trends. Focusing only on stage I (i.e. right hand-side of vertical dashed line), it can be concluded that the rapid stress change is governed by $\sigma_{z,b}$ and hence, by the deformation of the polymer backbone.

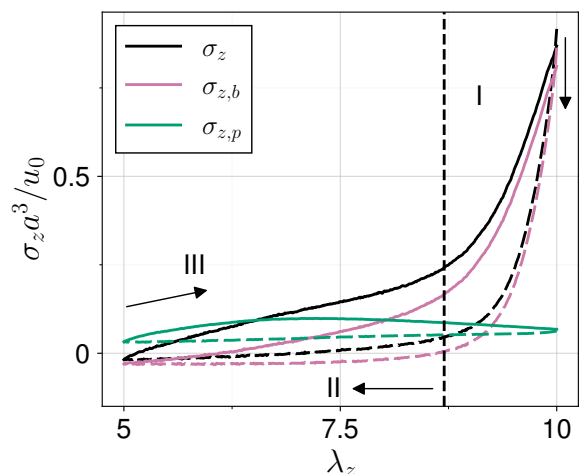


Figure 2: Axial stress σ_z decomposition into intermolecular pair $\sigma_{z,p}$ and intramolecular bond $\sigma_{z,b}$ components during unloading (dashed lines) and reloading (solid lines) for $\lambda_{z,u} = 5$. Arrows show load direction.

Since Figure 2 suggests that chain (re)orientation is important, we further analyze the changes in chain configuration by computing orientation vectors $\vec{R}(N_i, \lambda_z)$ between N_i beads along the chains for a given stretch λ_z . The average orientation of these vectors is conveniently described by

$$S_z = \langle P_2(\cos \alpha_z(N_i, \lambda_z)) \rangle, \quad (3)$$

where $P_2(x) = (3x^2 - 1)/2$ is the second Legendre polynomial, α_z the angle formed by

$\vec{R}(N_i, \lambda_z)$ with the deformation axis and $\langle \rangle$ describes the ensemble average. Figure 3 shows a parametric plot of the stress as function of S_z for five values of N_i , where $N_i = 80$ coincides with the entanglement length N_e .

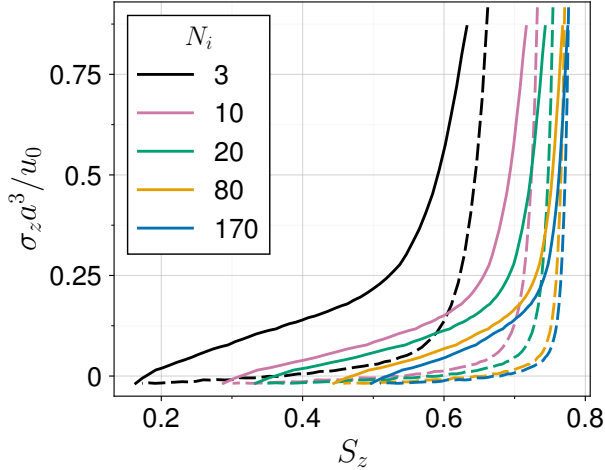


Figure 3: Axial stress σ_z vs. bond orientation S_z for several length scales encompassing N_i monomers. Data is shown during unloading (dashed lines) and reloading (solid lines) for $\lambda_{z,u} = 5$.

The first notable observation is that S_z is not an adequate order parameter at any length scale N_i to characterise the hysteresis, since the hysteresis loops do not collapse. Second, given that $S_z(N_i = 80) \approx S_z(N_i = 170)$, the orientation seems to be enforced by the entanglement network. Third, before unloading from $\lambda_{z,max}$, the chains are highly oriented, which is essentially retained during the initial stages of unloading (dashed lines) in which the stress rapidly decays. Lastly, the rapid stress rise during reloading (solid lines) in regime I is accompanied by a minor change in orientation.

The stretching and relaxing of the backbone bonds is further corroborated by Figure 4, which shows the average resultant tensile bond force $\langle F_b \rangle = \langle dU_{FENE}(r)/dr \rangle$. It closely follows the bond stress $\sigma_{z,b}$ derived from the virial stress, and paints the picture that constraints such as the entanglement network leads to a rise in σ_z once chains become highly oriented. Furthermore, upon unloading, the loss in entanglement contacts yields a swift stress relaxation in the backbone and thus causes the difference

in loading and unloading.

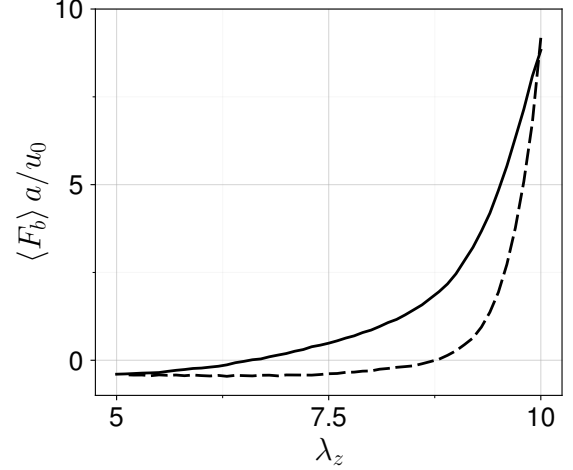


Figure 4: Average backbone bond force $\langle F_b \rangle$ vs. stretch λ_z during unloading (dashed lines) and reloading (solid lines) for $\lambda_{z,u} = 5$.

In conclusion, stage I is governed by the stretching and relaxing of the highly oriented bonds due to the entanglement network. As the bonds form craze fibrils, it equivalently can be stated that this stage is governed by the deformation of the highly oriented craze fibrils. Given the necessary pre-orientation in order for the deformation to take place, this stage is essentially independent of the prior unloading history (i.e. of $\lambda_{z,u}$).

3.1.2 Mechanics during stage II

Stage II focuses on the mechanisms leading to the quasi stress-free contraction of the craze during unloading as well as the transition to compression for $\lambda_z \leq 2.5$. The data presented so far highlights two things in this regime: Firstly, the largest reduction in chain orientation occurs during this stage (cf. Figure 3) and secondly, $\sigma_{z,b} \approx \langle F_b \rangle \approx 0$ (cf. Figure 2 and Figure 4). The latter suggests that the structural behaviour of craze fibrils is string-like rather than beam-like as the craze (pore space & fibrils) solely exhibits a minor stiffness during contraction. This also implies a negligible bending stiffness of the craze fibrils, which validates a recent assumption on the structural behaviour of craze fibrils used in a continuum model.³¹

Besides the chain level observables, a further helpful quantity to characterise the response

is the particle motion orthogonal (i.e. in xy -plane) to the deformation axis (z -axis). Since $\lambda_x = \lambda_y = 1$, any such motion is nonaffine. The average lateral particle displacement $\langle u_{xy} \rangle$ is given by

$$\langle u_{xy} \rangle = \langle |\vec{r}_{xy}(\tau_c) - \vec{r}_{xy}(\tau_c = 0)| \rangle, \quad (4)$$

where \vec{r}_{xy} is the position vector in the xy -plane and $\langle u_{xy} \rangle$ is the displacement with respect to $\lambda_{z,max}$ at the beginning of the cycle at $\tau_c = 0$. Figure 5 displays the evolution of $\langle u_{xy} \rangle$ (black line) as well as σ_z (magenta line) throughout the loading cycle. During unloading ($0 < \tau_c \leq 0.5$), $\langle u_{xy} \rangle$ increases sharply. That is, the lateral particle movement increases while the bond orientation decreases, which can also be seen in the supplementary animation as a "folding mechanism" of the craze fibrils. The pore space plays a key role as it enables the motion of fibril folding to occur essentially as a rigid body motion, i.e. stress-free. It is therefore concluded, that as long as pore space exists, the structural behaviour of craze fibrils is thus most accurately described as string-like.

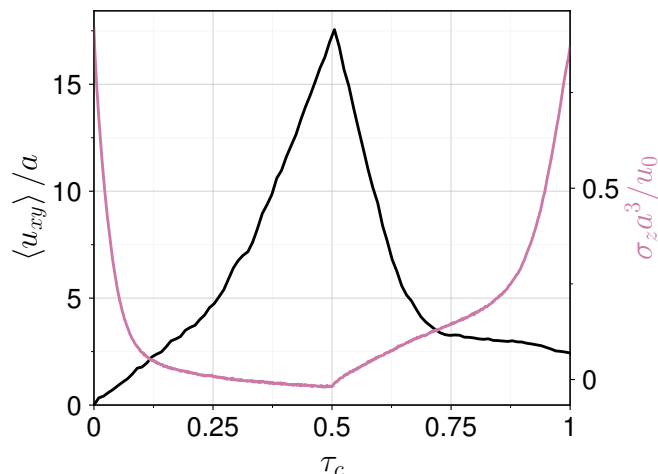


Figure 5: Lateral particle displacement $\langle u_{xy} \rangle$ (left y-axis) and σ_z (right y-axis) vs. cycle time τ_c for $\lambda_{z,u} = 5$.

The compressive stress increase observed for $\lambda_z \leq 2.5$ (cf. Figure 1(b)) arises from an increase in $\sigma_{z,p}$ (cf. stress decomposition of $\lambda_{z,u} = 1$ and $\lambda_{z,u} = 2$ in Figure S3). Although the magnitude is quite large and most likely strongly influenced by the high deformation speed in MD simulations, this behaviour is

not unexpected due to the macroscopically observed dilatant deformation during craze formation and growth, leading to compressive stress ($\sigma_z < 0$) during unloading while the macroscopic deformation is still tensile ($\lambda_z > 1$). Compression at the crack tip, i.e. where the craze is the largest, was also computed using the experimentally measured craze contour as input in a finite element simulation.^{30,40}

3.1.3 Mechanics during stage III

Stage III features the reloading response, which significantly depends on $\lambda_{z,u}$. The supplementary animations show that in the case of $\lambda_{z,u} = 5$, the craze morphology is largely retained throughout the cycles. By contrast, $\lambda_{z,u} = 2$ yields a section-wise unfolding of the craze and $\lambda_{z,u} = 1$ even a re-drawing. The previous data implies that pore space closure and the exerted compression highly influence the reloading behaviour. To further study the underlying mechanism that contributes especially to the difference between $\lambda_{z,u} = 2$ and $\lambda_{z,u} = 1$, the simulation box length L_z is decomposed into regions associated with the bulk material

$$L_b = \int_{\{z:\rho(\tau_c,z) \geq \rho_b\}} dz, \quad (5)$$

the craze

$$L_c = \int_{\{z:\rho(\tau_c,z) \leq \rho_c\}} dz \quad (6)$$

and an intermediate length

$$L_i = \int_{\{z:\rho_c < \rho(\tau_c,z) < \rho_b\}} dz, \quad (7)$$

where $\rho(\tau_c, z)$ is the density of a slab dz at τ_c and ρ_b and ρ_c are the bulk and craze density, respectively. The evolution of those craze length components is displayed in Figure 6, including additionally snapshots of the craze (created with OVITO³⁹) for the three simulations compressed to different $\lambda_{z,u}$ -values, and then restrained to the same $\lambda_z = 5$. To further facilitate the understanding of the approach, the area enclosed by the coloured dashed lines in snapshot Figure 6(a) defines the three contri-

butions associated with L_b , L_c and L_i .

In all three simulations, the simulation box consists solely of crazed material ($L_c = L_z$) at $\tau_c = 0$. As the deformation is retracted and the craze unloaded, L_i increases monotonically to L_z . In the case of $\lambda_{z,u} = 1$, the high compressive stress eventually leads to a very rapid increase from $L_b = 0$ to $L_b = 1$ (cf. green line around $\tau_c \approx 0.5$ in Figure 6(a)). Upon reloading, L_i quickly rises and subsequently L_b as well as L_i continuously decrease. This is associated with the re-drawing of fibrils as can be seen in the animation. The small rise of L_i can be understood as new "active zone" (magenta area shown in the Figure 6(a) snapshot), from which fibrils are drawn. In this context, it is important to realize that the decrease in L_i results merely from the normalisation, but is rather a constant active zone length (see Figure S5 in a non-normalised plot for L_i). We also note that it would be misleading to characterise this behaviour as healing of the craze, as neither the temperature nor the simulation time allows for any substantial chain reptation. The response arises rather from the breakage of intermolecular interactions, which were created during $\sigma_z < 0$ (cf. Figure S3(a)).

This behavior is in strong contrast to $\lambda_{z,u} \geq 2$, where L_b remains zero. While the key feature of $\lambda_{z,u} = 5$ is the retention of the craze morphology seen by smooth transitions between L_c and L_i in Figure 6(c), $\lambda_{z,u} = 2$ is more interesting. With the system reloading from $L_i = 1$ at $\tau_c = 0.5$ (Figure 6(b)), re-cavitation does not occur and the breaking of LJ interactions (cf. Figure S3(b)) results in a relatively constant plateau stress (cf. Figure 1(c)). The animation shows an "unfolding" behaviour of the craze, which can be seen by the evolution around $0.5 < \tau_c < 0.8$ in Figure 6(b). This becomes even more evident if the normalisation is omitted and L_i and L_c are plotted separately as shown in Figure S4.

3.2 Bulk-craze interaction

The study so far has focused on the cyclic deformation of fully crazed matter, which has been drawn from the isotropic glass. Yet, fibril draw-

ing is a transient process and hence it is also interesting to consider the cyclic response while craze and bulk material coexist. To investigate the role of the craze length, two configurations are created by deforming the initial glass to $\lambda_{z,max} = 5$ as well as $\lambda_{z,max} = 2$, leading to craze/bulk length ratios at $\lambda_{z,max}$ of $L_c/L_b = 9.8$ and $L_c/L_b = 1.3$, respectively. The protocol then follows the previous protocol by commencing the cyclic loading routine to three different $\lambda_{z,u}$ -values, leading to the bulk-craze interaction for the nine simulations shown in Figure 7. The deformation has been rescaled by $\varepsilon_z = (\lambda_z - 1)/(\lambda_{z,max} - 1)$, resulting in a collapse of the curves for a given unloading $\varepsilon_{z,u} = (\lambda_{z,u} - 1)/(\lambda_{z,max} - 1)$.

The bulk-craze interaction leads to a response very similar to the pure craze response in Figure 1 even for "short" crazes such as $L_c/L_b \approx 1$. This allows for two important conclusions: Firstly, the macro deformation is governed by the craze and the bulk plays a minor role in cyclic deformation. This is attributed to the much higher bulk stiffness E_b compared to the craze stiffness E_c . To further elaborate that, the bulk/craze stiffness can be crudely estimated by their respective secant stiffness with respect to λ_z while neglecting 3D effects. This yields $E_b/E_c \approx 100$, where E_b is evaluated at $\lambda_z = (1, 1.5)$ and E_c for reloading in regime I at $\lambda_z = (9.5, 10)$ in Figure 1(c). It is important to acknowledge that this is the craze stiffness and not the craze fibril stiffness. Secondly, the stress free contraction occurring also for shorter craze fibrils corroborates a negligible bending stiffness and hence the string-like structural response of craze fibrils.

We conclude this section by discussing an estimate of the craze length ξ_0 at $\lambda_{z,max}$. This estimate is limited to the case without pore space closure (i.e. $\varepsilon_z \geq 0.25$), which is then motivated by the scaling in Figure 7. While drawing is not exhausted, the craze essentially exhibits a layered bulk-craze structure at $\lambda_{z,max}$ in which the deformed craze layer is denoted by ξ and the deformed bulk layer by χ . They differ from L_c and L_b as ξ and χ are calculated in the following and not given by the MD simulations. Using further continuum micromechanical arguments (for de-

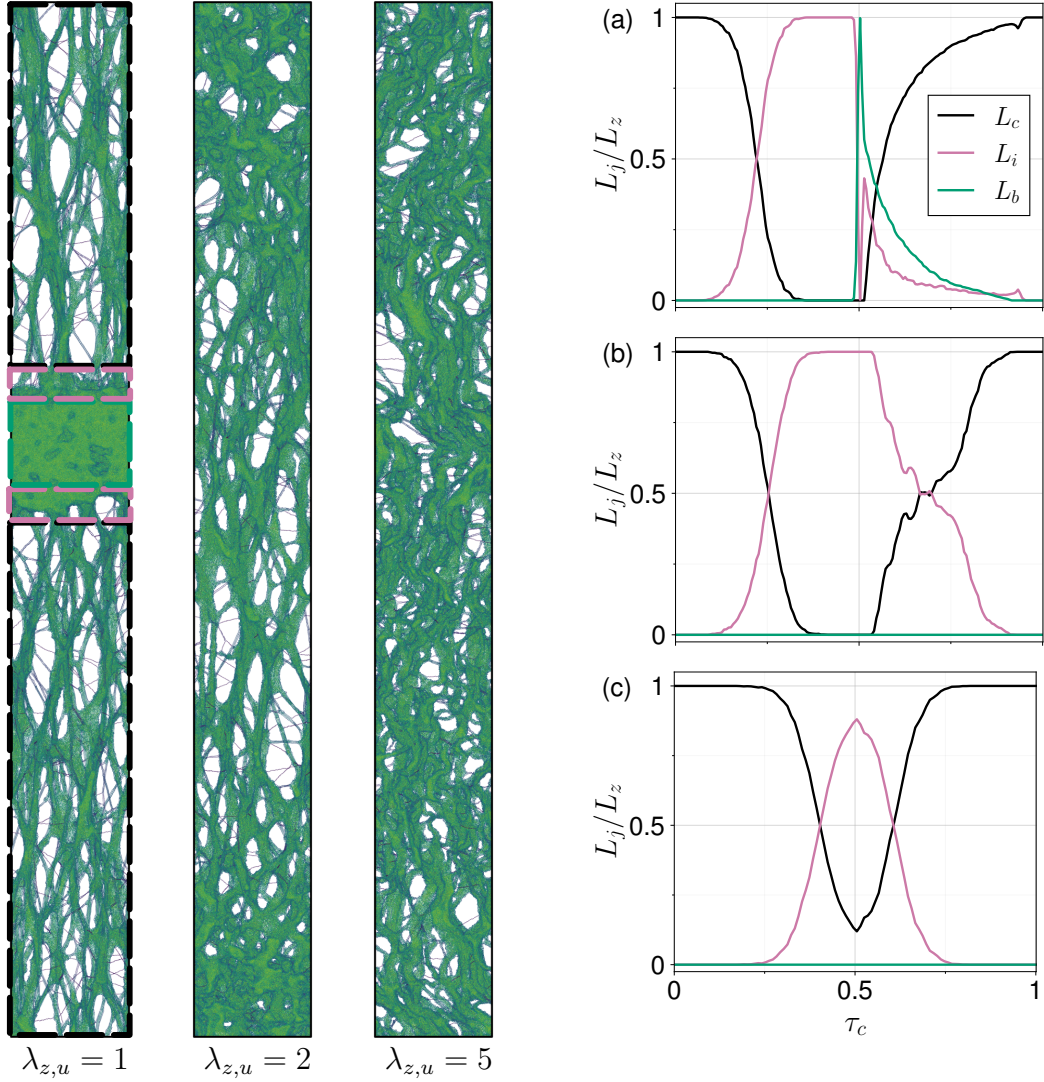


Figure 6: Snapshots of crazes during reloading at $\lambda_z = 5$ and corresponding evolution of craze length components throughout cycle for (a) $\lambda_{z,u} = 1$, (b) $\lambda_{z,u} = 2$ and (c) $\lambda_{z,u} = 5$.

tails including finite strains see³¹) yields the kinematic coupling between the macro stretch λ_z and the layers ξ and χ as

$$\lambda_z = \frac{\chi + \xi}{h_0}, \quad (8)$$

where $h_0 = L_{z0}$ is the primordial thickness. Furthermore, the unloaded bulk χ_0 and craze length ξ_0 are related by conservation of mass during the drawing process, given by

$$\chi_0 = h_0 - \xi_0/\lambda_c, \quad (9)$$

where λ_c is the extension ratio with respect to the unloaded configuration. To combine (8) and (9) without proposing constitutive deformation models, we assume small (elastic) deformations

of the bulk and craze, i.e. $\chi_0 \approx \chi$ and $\xi_0 \approx \xi$, allowing to derive an estimation for the craze fibril length

$$\xi_0 = h_0(\lambda_{z,max} - 1) \frac{\lambda_c}{\lambda_c - 1} \quad (10)$$

at $\lambda_{z,max}$. Applying (10) to $\lambda_{z,max} = 5$ and $\lambda_{z,max} = 2$ leads to $\xi_0/\chi_0 = 10$ and $\xi_0/\chi_0 = 1.3$, respectively, which is in good agreement with L_c/L_b values given by the MD simulations.

As a final remark, it is noteworthy that no continuous drawing is observed on the investigated time scales, which would be an indication for viscous drawing or viscous deformation effects of the fibril.

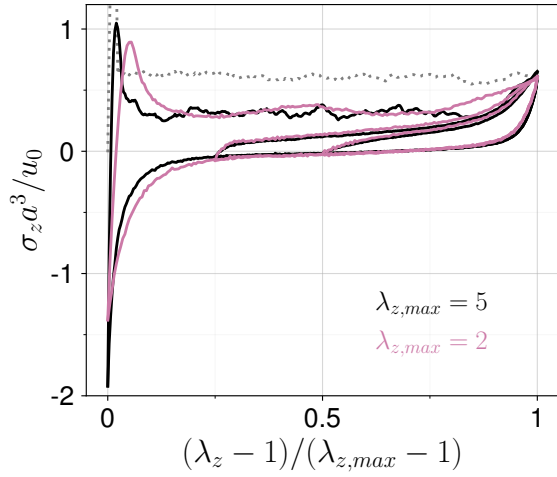


Figure 7: Stress-strain curves for two bulk-craze configurations obtained by $\lambda_{z,max} = 5$ (black lines) and $\lambda_{z,max} = 2$ (magenta lines) as well as the initial craze formation (grey dotted line). Each configuration features three unloading levels $\lambda_{z,u}$.

4 Conclusions

Molecular dynamics simulations were used to study the mechanical response of sole fibrillated craze matter and the bulk-craze interaction in glassy polymers under cyclic loading. The maximum loading amplitude $\lambda_{z,max}$ and unloading magnitude $\lambda_{z,u}$ were varied to simulate different bulk-craze compositions and different degrees of pore space closure, respectively. A key finding of this study was that in all investigated cases, i.e. the sole craze and the craze-bulk system, the macro responses exhibited a hysteresis, which was found to be quasi stationary after the first cycle and largely independent of deformation rate and temperature.

Another salient finding was that the hysteresis cannot be simply described by the chain orientation S_z , but rather resulted from a complex interplay between constraints imposed by the entanglement network, pore space and pore space closure. Three distinct craze stages were identified to study the driving mechanism in detail: The first stage focused on the highly oriented bonds and craze fibrils. Further deformation led to an accelerated increase in stress σ_z (cf. Figure 1), which resulted from the stretching of the covalent backbone bonds. Upon unloading the oriented craze, the bond force $\langle F_b \rangle$

quickly relaxed due to the loss in entanglement contact, yielding a rapid drop in σ_z . The second stage characterised the stress-free contraction during further unloading, in which the animations showed that the craze fibrils undergo a folding motion. The folding motion was characterised on the chain and particle level observables by a decrease in chain orientation and elevated lateral particle movement, respectively. The surrounding pore space is the essential trait for the folding motion to take place as a rigid body motion (i.e. stress-free). The third stage described the reloading response, which exhibited a strong dependency on $\lambda_{z,u}$. It was shown that a key feature is the degree of pore space closure and the necessary intermolecular interaction to enforce it. Complete pore space closure ($\lambda_{z,u} = 1$) was accompanied by a high level of intermolecular stress, which led to a re-cavitation and re-drawing during reloading. If the pore space was maintained throughout the cyclic (e.g. $\lambda_{z,u} = 5$), the reloading response was bi-linear.

The study on the craze-bulk interaction revealed that even "short" craze fibrils, where $L_b \approx L_c$, exhibited the three characteristic stages of sole fibrillated craze matter described above. That is, once a craze initiates and reaches a certain length, the macroscopic response is governed by the craze. This was attributed to the significantly lower craze stiffness (with respect to λ_z) of $E_b/E_c \approx 100$. It also allows to use continuum micromechanical considerations to estimate the craze-bulk ratio at peak loading.

A further important finding, there has not been an indication of a macroscopic bending stiffness during unloading, even in the case of "short" craze fibrils. The folding motion occurs on the craze fibril level which comprises locally stiff craze fibril segments (cf. animations). Therefore, it is likely that the results qualitatively hold for semiflexible bead-spring models, i.e. with a bending potential. While such models primarily yield a higher entanglement density, the crazing process is still dilatant by creating pore space and hence, the mechanisms leading to the stress-free contraction of the craze are still present. Concluding, the macroscopic

structural response of craze fibrils during unloading is most accurately described as string-like, despite locally stiff craze fibril segments. This finding is important, since a craze fibril bending stiffness would have different implications on the damage mechanisms during cyclic (fatigue) loading.

The most interesting contribution for future work includes carefully conducted experiments on fibrillated craze matter investigating the response under different loading conditions.

Acknowledgement We thank Siteng Zhang for providing the equilibrated melt configuration. Partial work was performed throughout a research stay of TL at the University of British Columbia, which was financially supported by the Karlsruhe House of Young Scientists (KHYS). Computational support from the state of Baden-Württemberg through bwHPC is gratefully acknowledged.

Supporting Information Available

The file (PDF) contains details on the animations and additional data presenting

- influence of deformation rate and temperature,
- stress evolution for multiple loading cycles,
- stress decomposition for $\lambda_{z,u} = 1$ and $\lambda_{z,u} = 2$ and
- evolution of craze length components for $\lambda_{z,u} = 1$ and $\lambda_{z,u} = 2$ in a non-normalised manner

MS1: Animation visualizing the cyclic craze response for $\lambda_{z,u} = 1$ (MP4)

MS2: Animation visualizing the cyclic craze response for $\lambda_{z,u} = 2$ (MP4)

MS3: Animation visualizing the cyclic craze response for $\lambda_{z,u} = 5$ (MP4)

References

- (1) Kramer, E. J.; Berger, L. L. In *Crazing in Polymers*; Kausch, H. H., Ed.; Advances in Polymer Science; Springer and Central Book Services New Zealand [distributor]: Berlin and Mitcham, VIC, Australia, 1990; Vol. 91/92; pp 1–68.
- (2) Kambour, R. P. A review of crazing and fracture in thermoplastics. *Journal of Polymer Science: Macromolecular Reviews* **1973**, *7*, 1–154.
- (3) Kausch, H.-H., Ed. *Crazing in polymers*; Advances in Polymer Science; Springer: Berlin, 1983; Vol. 52/53.
- (4) Kausch, H. H., Ed. *Crazing in Polymers*; Advances in Polymer Science; Springer and Central Book Services New Zealand [distributor]: Berlin and Mitcham, VIC, Australia, 1990.
- (5) Haward, R. N.; Young, R. J. *The Physics of Glassy Polymers*; Springer Netherlands: Dordrecht, 1997.
- (6) Tijssens, M.; van der Giessen, E.; Sluys, L. J. Modeling of crazing using a cohesive surface methodology. *Mechanics of Materials* **2000**, *32*, 19–35.
- (7) Estevez, R.; Tijssens, M.; van der Giessen, E. Modeling of the competition between shear yielding and crazing in glassy polymers. *Journal of the Mechanics and Physics of Solids* **2000**, *48*, 2585–2617.
- (8) Socrate, S.; Boyce, M. C.; Lazzeri, A. A micromechanical model for multiple crazing in high impact polystyrene. *Mechanics of Materials* **2001**, *33*, 155–175.
- (9) Gearing, B. P.; Anand, L. On modeling the deformation and fracture response of glassy polymers due to shear-yielding and crazing. *International Journal of Solids and Structures* **2004**, *41*, 3125–3150.

- (10) Basu, S.; Mahajan, D. K.; van der Giessen, E. Micromechanics of the growth of a craze fibril in glassy polymers. *Polymer* **2005**, *46*, 7504–7518.
- (11) Seelig, T. Computational modeling of deformation mechanisms and failure in thermoplastic multilayer composites. *Composites Science and Technology* **2008**, *68*, 1198–1208.
- (12) Helbig, M.; van der Giessen, E.; Clausen, A. H.; Seelig, T. Continuum-micromechanical modeling of distributed crazing in rubber-toughened polymers. *European Journal of Mechanics - A/Solids* **2016**, *57*, 108–120.
- (13) Baljon, A. R. C.; Robbins, M. O. Simulations of Crazing in Polymer Glasses: Effect of Chain Length and Surface Tension. *Macromolecules* **2001**, *34*, 4200–4209.
- (14) Rottler, J.; Robbins, M. O. Jamming under Tension in Polymer Crazes. *Phys. Rev. Lett.* **2002**, *89*, 195501.
- (15) Rottler, J.; Barsky, S.; Robbins, M. O. Cracks and Crazes: On Calculating the Macroscopic Fracture Energy of Glassy Polymers from Molecular Simulations. *Phys. Rev. Lett.* **2002**, *89*, 148304.
- (16) Rottler, J.; Robbins, M. O. Growth, microstructure, and failure of crazes in glassy polymers. *Physical review. E, Statistical, nonlinear, and soft matter physics* **2003**, *68*, 011801.
- (17) Mahajan, D. K.; Singh, B.; Basu, S. Void nucleation and disentanglement in glassy amorphous polymers. *Phys. Rev. E* **2010**, *82*, 011803.
- (18) Toepperwein, G. N.; de Pablo, J. J. Cavitation and Crazing in Rod-Containing Nanocomposites. *Macromolecules* **2011**, *44*, 5498–5509.
- (19) Mahajan, D. K.; Hartmaier, A. Mechanisms of crazing in glassy polymers revealed by molecular dynamics simulations. *Phys. Rev. E* **2012**, *86*, 021802.
- (20) Venkatesan, S.; Basu, S. Investigations into crazing in glassy amorphous polymers through molecular dynamics simulations. *Journal of the Mechanics and Physics of Solids* **2015**, *77*, 123–145.
- (21) Ge, T.; Grest, G. S.; Robbins, M. O. Tensile Fracture of Welded Polymer Interfaces: Miscibility, Entanglements, and Crazing. *Macromolecules* **2014**, *47*, 6982–6989.
- (22) Ge, T.; Tzoumanekas, C.; Anogiannakis, S. D.; Hoy, R. S.; Robbins, M. O. Entanglements in Glassy Polymer Crazing: Cross-Links or Tubes? *Macromolecules* **2017**, *50*, 459–471.
- (23) Wang, J.; in 't Veld, P. J.; Robbins, M. O.; Ge, T. Effects of Coarse-Graining on Molecular Simulation of Craze Formation in Polymer Glass. *Macromolecules* **2022**, *55*, 1267–1278.
- (24) Dietz, J. D.; Nan, K.; Hoy, R. S. Unexpected Ductility in Semiflexible Polymer Glasses with Entanglement Length Equal to Their Kuhn Length. *Phys. Rev. Lett.* **2022**, *129*, 127801.
- (25) Nan, K.; Hoy, R. S. Craze Extension Ratio of Semiflexible Polymer Glasses. *Macromolecules* **2023**, *56*, 8369–8375.
- (26) Döll, W.; Könczöl, L. In *Crazing in Polymers*; Kausch, H. H., Ed.; Advances in Polymer Science; Springer and Central Book Services New Zealand [distributor]: Berlin and Mitcham, VIC, Australia, 1990; Vol. 91/92; pp 137–214.
- (27) Schirrer, R. In *Crazing in Polymers Vol. 2*; Kausch, H. H., Ed.; Springer Berlin Heidelberg: Berlin, Heidelberg, 1990; pp 215–261.
- (28) Takemori, M. T. In *Crazing in Polymers*; Kausch, H. H., Ed.; Advances in Polymer Science; Springer and Central Book Services New Zealand [distributor]: Berlin and Mitcham, VIC, Australia, 1990; Vol. 91/92; pp 263–300.

- (29) Skibo, M. D.; Hertzberg, R. W.; Manson, J. A.; Kim, S. L. On the generality of discontinuous fatigue crack growth in glassy polymers. *Journal of Materials Science* **1977**, *12*, 531–542.
- (30) Könczöl, L.; Döll, W.; Bevan, L. Mechanisms and micromechanics of fatigue crack propagation in glassy thermoplastics. *Colloid & Polymer Science* **1990**, *268*, 814–822.
- (31) Laschuetza, T.; Seelig, T. A continuum-micromechanical model for crazing in glassy polymers under cyclic loading. *Mechanics of Materials* **2024**, *189*, 104901.
- (32) Kambour, R. P.; Kopp, R. W. Cyclic stress–strain behavior of the dry polycarbonate craze. *Journal of Polymer Science Part A-2: Polymer Physics* **1969**, *7*, 183–200.
- (33) Hoare, J.; Hull, D. Craze yielding and stress-strain characteristics of crazes in polystyrene. *The Philosophical Magazine: A Journal of Theoretical Experimental and Applied Physics* **1972**, *26*, 443–455.
- (34) Kremer, K.; Grest, G. S. Dynamics of entangled linear polymer melts: A molecular-dynamics simulation. *The Journal of Chemical Physics* **1990**, *92*, 5057–5086.
- (35) Plimpton, S. Fast Parallel Algorithms for Short-Range Molecular Dynamics. *Journal of Computational Physics* **1995**, *117*, 1–19.
- (36) Thompson, A. P.; Aktulga, H. M.; Berger, R.; Bolintineanu, D. S.; Brown, W. M.; Crozier, P. S.; in 't Veld, P. J.; Kohlmeyer, A.; Moore, S. G.; Nguyen, T. D.; Shan, R.; Stevens, M. J.; Tranchida, J.; Trott, C.; Plimpton, S. J. LAMMPS - a flexible simulation tool for particle-based materials modeling at the atomic, meso, and continuum scales. *Comp. Phys. Comm.* **2022**, *271*, 108171.
- (37) Auhl, R.; Everaers, R.; Grest, G. S.; Kremer, K.; Plimpton, S. J. Equilibration of long chain polymer melts in computer simulations. *The Journal of Chemical Physics* **2003**, *119*, 12718–12728.
- (38) Hoy, R. S.; Robbins, M. O. Effect of equilibration on primitive path analyses of entangled polymers. *Phys. Rev. E* **2005**, *72*, 061802.
- (39) Stukowski, A. Visualization and analysis of atomistic simulation data with OVITO—the Open Visualization Tool. *Modelling and Simulation in Materials Science and Engineering* **2009**, *18*, 015012.
- (40) Bevan, L.; Doell, W.; Koenczoel, L. Micromechanics of a craze zone at the tip of a stationary crack. *Journal of Polymer Science Part B: Polymer Physics* **1986**, *24*, 2433–2444.

TOC Graphic

